SPECTRAL ANALYSIS OF A BLOCK-TRIANGULAR PRECONDITIONER FOR THE BIDOMAIN SYSTEM IN ELECTROCARDIOLOGY

LUCA GERARDO-GIORDA AND LUCIA MIRABELLA

Abstract. In this paper we analyse in detail the spectral properties of the block-triangular preconditioner for the Bidomain system in non-symmetric form, introduced in [8]. We show that the conditioning of the preconditioned problem is bounded, in the Fourier space, independently from the frequency variable, ensuring quasi optimality with respect to the mesh size. We derive an explicit formula to optimize the preconditioner performance, by identifying a parameter that depends only on the coefficients of the problem and is easy to compute. We provide numerical tests in three dimensions that confirm the optimality of the parameter and the substantial independence from the mesh size.

1. Introduction

The Bidomain model is commonly considered one of the most complete and accurate models to describe the propagation of the electrical potential in the myocardium tissue (see e.g.[19], [26], [22], [10]). It consists of a system of nonlinear unsteady partial differential equations governing the dynamics of intra and extracellular potentials, coupled with a system of ODEs that describes the dynamics of membrane currents. The discretization of the Bidomain model is often based on a finite element approximation in space and on implicit-explicit time advancing schemes, that allow to skip the expensive solution of nonlinear systems. The degenerate parabolic nature of this system, however, entails a very ill conditioning for the linear system associated to the Bidomain discretization. Several scientists have developed in the recent years effective preconditioning strategies to reduce the high computational costs associated to its numerical solution ([5], [14], [13], [31], [16], [17], [30], [28], [27]). Among these works, most are based on a proper decomposition of the computational domain in order to set up parallel preconditioners, or on suitable multigrid schemes still coupled with parallel architectures. An efficient serial preconditioner has been proposed in [8] stemming from a suitable adaptation of the Monodomain model. The latter is a simplified model that is based on a (quite unrealistic) proportionality assumption between the intra and extracellular conductivity tensors, and consists of a single parabolic equation for the transmembrane potential: if on the one hand it is computationally very cheap, on the other hand is not able to capture significant patterns of excitation and repolarization in both physiological and pathological conditions. However, a suitable extension of the Monodomain model resulted in a lower block-triangular preconditioner for a nonstandard formulation of the Bidomain model ([8]): the preconditioner proved to be very effective and robust with respect to the mesh size in terms of both iteration counts and CPU time, but an accurate theoretical analysis of the preconditioner was not carried out in there. Aside, the preconditioner depends upon the choice of a parameter λ that in [8] was tuned empirically. This paper is devoted to an accurate spectral analysis of the block-triangular preconditioner proposed in [8]: by means of Fourier analysis we enlighten the optimality of the preconditioner with respect to the mesh size, and we provide a formula to identify an optimal parameter λ^*.

The paper is organized as follows. In Section 2 we introduce the Bidomain model and its non-symmetric formulation. Section 3 is devoted to present the numerical discretization and the block-triangular preconditioner at the discrete level. In Section 4 we carry out the spectral analysis of the preconditioner, and we provide a formula for the optimal parameter λ^*. In Section 5 we extend our analysis to the symmetric parabolic-elliptic formulation of the Bidomain system. Finally, in Section 6 we provide some numerical results in three dimensions to illustrate our findings.

2. The Bidomain model

The myocardial tissue is composed of elongated cells, the *cardiac fibers*, connected each other by gap junctions and surrounded by an extracellular medium. From a mathematical point of view, this structure can be modeled as a continuum in which the electrical variables are obtained as the average of the single cell properties, after a homogenization process ([7], [20], [15], [3]). The cardiac tissue can be represented as a superposition of intra and extracellular media connected by a cell membrane dislocated in the domain. The Bidomain model should take into account the direction of the cardiac fibers. Anatomical studies show that the fibers direction rotates counterclockwise from epicardium to endocardium and that they are arranged in sheets, running across the myocardial wall ([9], [12], [26]). We set the problem in a bounded region $\Omega \subset \mathbb{R}^3$, and we assume that the cardiac tissue is characterized at each point by three directions: $\boldsymbol{a}_l$ along the fiber, $\boldsymbol{a}_t$ orthogonal to the fiber direction and in the fiber sheet and $\boldsymbol{a}_n$ orthogonal to the sheet. The intra and extracellular media present different conductivity values in each direction. We denote by $\sigma_i^l(\boldsymbol{x})$ (resp. $\sigma_e^l(\boldsymbol{x})$) the intracellular (resp. extracellular) conductivity in $\boldsymbol{a}_l(\boldsymbol{x})$ direction at point $\boldsymbol{x} \in \Omega$, and similarly by $\sigma_i^t(\boldsymbol{x})$ ($\sigma_e^t(\boldsymbol{x})$) and $\sigma_i^n(\boldsymbol{x})$ ($\sigma_e^n(\boldsymbol{x})$) the conductivities along $\boldsymbol{a}_t(\boldsymbol{x})$ and $\boldsymbol{a}_n(\boldsymbol{x})$. We will use throughout the paper the notation $\sigma_\tau^l(\boldsymbol{x})$, $\sigma_\tau^n(\boldsymbol{x})$, $\sigma_\tau^t(\boldsymbol{x})$ with $\tau = i, e$ for indicating intra and extracellular conductivity in a compact form.

The intra and extracellular local anisotropic conductivity tensors read therefore

$$\mathbf{D}_\tau(\boldsymbol{x}) = \sigma_\tau^l(\boldsymbol{x})\boldsymbol{a}_l(\boldsymbol{x})\boldsymbol{a}_l^T(\boldsymbol{x}) + \sigma_\tau^t(\boldsymbol{x})\boldsymbol{a}_t(\boldsymbol{x})\boldsymbol{a}_t^T(\boldsymbol{x}) + \sigma_\tau^n(\boldsymbol{x})\boldsymbol{a}_n(\boldsymbol{x})\boldsymbol{a}_n^T(\boldsymbol{x}) \tag{1}$$

for $\tau = i, e$. We assume that $\mathbf{D}_\tau$ fulfills in Ω a uniform elliptic condition. In this paper, following [5], we also assume axial isotropy for the myocardium, amounting to show the same conductivity in both the tangential and normal direction. Under this hypotesis, the tensors simplify in

$$\mathbf{D}_\tau(\boldsymbol{x}) = \sigma_\tau^t\mathbf{I} + (\sigma_\tau^l - \sigma_\tau^t)\boldsymbol{a}_l(\boldsymbol{x})\boldsymbol{a}_l^T(\boldsymbol{x}) \tag{2}$$

for $\tau = i, e$.

Let u_i and u_e be the intra and extracellular potentials respectively and $u = u_i - u_e$ be the transmembrane potential. The density current in each domain can be computed as $\mathbf{J}_\tau = -\mathbf{D}_\tau \nabla u_\tau$, $\tau = i, e$. The net current flux between the intra and the extracellular domain is assumed to be zero as a consequence of the charge conservation in an arbitrary portion of tissue. Denoting by I_m the ingoing membrane current flow and by χ the ratio of membrane area per tissue volume, we get $\nabla \cdot (\mathbf{D}_i \nabla u_i) = \chi I_m = -\nabla \cdot (\mathbf{D}_e \nabla u_e)$, where $I_m = C_m \partial_t u + I_{ion}(u, \boldsymbol{w})$ being C_m a capacitance and I_{ion} the ionic current, depending on the potential u and on suitable ionic variables that we denote with $\boldsymbol{w}$. The complete Bidomain model reads

$$\begin{cases} \chi C_m \partial_t u - \nabla \cdot \mathbf{D}_i \nabla u_i + \chi I_{\text{ion}}(u, \boldsymbol{w}) = \quad I_i^{\text{app}} \\ \\ -\chi C_m \partial_t u - \nabla \cdot \mathbf{D}_e \nabla u_e - \chi I_{\text{ion}}(u, \boldsymbol{w}) = -I_e^{\text{app}} \end{cases} \tag{3}$$

where $I_{\text{ion}}(u, \boldsymbol{w})$ is a nonlinear function of the transmembrane potential u, specified by a ionic model, and where $I_{i,e}^{\text{app}}$ are applied external stimuli. In what follows we do not rely on a specific choice for the ionic model describing the cell membrane currents (thus from now on we simply denote by $I_{\text{ion}}(u)$ the ionic current). In our numerical tests we consider as models for ventricular

cells both the Luo-Rudy Phase 1 model [24], and the Rogers-McCulloch variant of the FitzHugh-Nagumo model [21]. The problem is completed by initial conditions, $u_i(\boldsymbol{x},0) = u_{i,0}, u_e(\boldsymbol{x},0) = u_{e,0}$, $u(\boldsymbol{x},0) = u_{i,0} - u_{e,0}$ and by homogeneous Neumann boundary conditions on $\partial\Omega$, modeling an insulated myocardium,

$$\mathbf{n}^T\mathbf{D}_i\nabla u_i(\boldsymbol{x},t) = 0 \quad \text{and} \quad \mathbf{n}^T\mathbf{D}_e\nabla u_e(\boldsymbol{x},t) = 0, \quad \text{on } \partial\Omega\times(0,T), \tag{4}$$

where $\mathbf{n}$ is the unit normal outward-pointing vector on the surface. As a consequence of the Gauss theorem, the applied external stimuli must fulfill the compatibility condition

$$\int_\Omega I_i^{\text{app}}\,d\boldsymbol{x} = \int_\Omega I_e^{\text{app}}\,d\boldsymbol{x}. \tag{5}$$

System (3) consists of two parabolic reaction diffusion equations for u_i and u_e where the vector of time derivatives is multiplied by a singular matrix. The system is thus said to be *degenerate*. The transmembrane potential u is uniquely determined, while the intra and extracellular potentials u_i and u_e are determined up to the same function of time, whose value is usually obtained by imposing that u_e has zero mean on Ω. For well-posedeness analysis of the Bidomain problem see [7] (Fitzugh-Nagumo model) and [29] (Luo-Rudy I model).
In what follows we will rely on a non-symmetric formulation of (3) (see e.g. [11], [8]). In that order, we define

$$\lambda_m = \min\left\{\frac{\sigma_e^l}{\sigma_i^l}, \frac{\sigma_e^t}{\sigma_i^t}\right\} \qquad \lambda_M = \max\left\{\frac{\sigma_e^l}{\sigma_i^l}, \frac{\sigma_e^t}{\sigma_i^t}\right\}. \tag{6}$$

By linear combinations of the two equations in (3), with coefficients $\left(\frac{\lambda}{1+\lambda}, -\frac{1}{1+\lambda}\right)$, with $\lambda_m \le \lambda \le \lambda_M$, and $(1,1)$, the Bidomain system can be reformulated in terms of the transmembrane and the extracellular potentials u and u_e as

$$\begin{cases} \chi C_m\dfrac{\partial u}{\partial t} - \nabla\cdot\left[\dfrac{\lambda\mathbf{D}_i}{1+\lambda}\nabla u\right] - \nabla\cdot\left[\dfrac{\lambda\mathbf{D}_i - \mathbf{D}_e}{1+\lambda}\nabla u_e\right] + \chi I_{ion}(u) = I^{\text{app}} \\ \\ -\nabla\cdot[\mathbf{D}_i\nabla u + (\mathbf{D}_i+\mathbf{D}_e)\nabla u_e] = \widetilde{I}^{\text{app}}, \end{cases} \tag{7}$$

where we have set $I^{\text{app}} = \dfrac{\lambda I_i^{\text{app}} + I_e^{\text{app}}}{1+\lambda}$ and $\widetilde{I}^{\text{app}} = I_i^{\text{app}} - I_e^{\text{app}}$.

3. Numerical approximation and the block-triangular preconditioner

We give a quick glance to the numerical approximation of the Bidomain model and to the block-triangular preconditioner. For a more detailed description see for instance [5, 20, 31], and [8], respectively.

3.1. Finite dimensional formulation.

For sake of presentation, we consider a time advancing procedure with fixed step Δt, and we denote with the superscript n the variables computed at time $t^n = n\Delta t$. Time adaptive scheme have been considered (see e.g. [4, 18]) but, on the one hand their analysis goes beyond the scope of this paper, and on the other hand a fixed time step does not affect the generality of the present analysis.
The Bidomain equations (7) can be advanced in time by a semi-implicit scheme, where the nonlinear term (the ionic current) is evaluated at the previous time steps. More precisely, moving from time

step t^n to t^{n+1} we solve on Ω

$$
\begin{cases}
\chi C_m \dfrac{u^{n+1}-u^n}{\Delta t} - \nabla\cdot\left[\dfrac{\lambda\mathbf{D}_i}{1+\lambda}\nabla u^{n+1} + \dfrac{\lambda\mathbf{D}_i-\mathbf{D}_e}{1+\lambda}\nabla u_e^{n+1}\right] = I^{\rm app} - \chi I_{ion}(u^n) \\
-\nabla\cdot\left[\mathbf{D}_i\nabla u^{n+1} + (\mathbf{D}_i+\mathbf{D}_e)\nabla u_e^{n+1}\right] = \widetilde{I}^{\rm app} \\
u^0(\boldsymbol{x}) = u_0(\boldsymbol{x}) \qquad u_e^0(\boldsymbol{x}) = u_{e,0}(\boldsymbol{x}) \\
\mathbf{n}^T\mathbf{D}_i(\nabla u^{n+1} + \nabla u_e^{n+1})|_{\partial\Omega} = 0 \qquad \mathbf{n}^T\mathbf{D}_e\nabla u_e^{n+1}|_{\partial\Omega} = 0.
\end{cases} \tag{8}
$$

We denote $f^n = I^{\rm app} - \chi I_{ion}(u^n) + \dfrac{\chi C_m}{\Delta t}u^n$ and $g = \widetilde{I}^{\rm app}$. In the sequel, when the context is clear we will drop the time index $n+1$.
We discretize in space the domain with a regular triangulation $\mathcal{T}_h$ and we consider a finite element space V_h, in which we will look for the approximate solutions, namely u^h and u_e^h. For the numerical tests in Section 6, V_h is the space of piecewise linear continuous functions on $\mathcal{T}_h$.
We denote by $\Phi = \{\varphi_j\}_{j=1}^{N_h}$ a basis for V_h, by $\mathcal{M}$ the mass matrix with entries $\mathcal{M}^{ij} = \sum_{K\in\mathcal{T}_h}(\varphi_j,\varphi_i)|_K$, and by $\mathcal{K}_\tau$ $(\tau = i, e)$ the stiffness matrices with $\mathcal{K}_\tau^{ij} = \sum_{K\in\mathcal{T}_h}(\mathbf{D}_\tau\nabla\varphi_j,\nabla\varphi_i)|_K$, $\varphi_i,\ \varphi_j \in \Phi$.
When solving the Bidomain system, the unknowns of the fully discrete problem are represented by vectors $\mathbf{u}$ and $\mathbf{u}_e$, storing the nodal values of u^h and u_e^h, respectively, we let $\mathbf{f}^n$ and $\mathbf{g}$ denote the discretization of the forcing terms, and we set

$$
\mathbf{B}_{uu} = \frac{\chi C_m}{\Delta t}\,\mathcal{M} + \frac{\lambda}{1+\lambda}\,\mathcal{K}_i \qquad \mathbf{B}_{ue} = \frac{\lambda}{1+\lambda}\,\mathcal{K}_i - \frac{1}{1+\lambda}\,\mathcal{K}_e \qquad \mathbf{B}_{eu} = \mathcal{K}_i \qquad \mathbf{B}_{ee} = \mathcal{K}_i + \mathcal{K}_e.
$$

At step t^{n+1} the discrete Bidomain models solves

$$
\mathbf{B}\,\mathbf{x}^{n+1} = \mathbf{h}^n, \tag{9}
$$

where

$$
\mathbf{B} = \begin{bmatrix} \mathbf{B}_{uu} & \mathbf{B}_{ue} \\ \mathbf{B}_{eu} & \mathbf{B}_{ee} \end{bmatrix}, \qquad \mathbf{x} = \begin{bmatrix} \mathbf{u} \\ \mathbf{u}_e \end{bmatrix}, \qquad \mathbf{h} = \begin{bmatrix} \mathbf{f} \\ \mathbf{g} \end{bmatrix}. \tag{10}
$$

Since the Bidomain system (3) is degenerate, the matrix $\mathbf{B}$ in its discrete formulation is singular, with a kernel spanned by the constants. We thus solve (9) with an iterative method (GMRES) and we force a zero mean value on the extracellular potential by imposing $\mathbf{1}^T\mathcal{M}\mathbf{u}_e = 0$.

3.2. **The Block-GS preconditioner and the Monodomain model.** The discrete Bidomain system (9) is preconditioned by a block-Gauss-Seidel strategy, relying on its lower block-triangular part

$$
\mathbf{M} = \begin{bmatrix} \mathbf{B}_{uu} & \mathbf{0} \\ \mathbf{B}_{eu} & \mathbf{B}_{ee} \end{bmatrix}.
$$

The derivation of such preconditioner from a model-based approximation is described in [8] and we will not dwell here upon it. We only point out that the matrix $\mathbf{M}$ arises from assuming $\mathbf{D}_e = \lambda\mathbf{D}_i$ in the first equation of (7), and corresponds to the discretization of the Extended Monodomain system

$$
\begin{cases}
\chi C_m \dfrac{\partial u}{\partial t} - \nabla\cdot\left(\dfrac{\lambda\mathbf{D}_i}{1+\lambda}\nabla u\right) + \chi I_{ion}(u,\boldsymbol{w}) = I^{\rm app} \\
-\nabla\cdot\left[\mathbf{D}_i\nabla u + (1+\lambda)\mathbf{D}_i\nabla u_e\right] = \widetilde{I}^{\rm app}.
\end{cases} \tag{11}
$$

coupled with Neumann boundary conditions (see [8]).
At the generic time step, we thus solve the preconditioned problem

$$\mathbf{M}^{-1}\mathbf{B}\mathbf{x}^{n+1} = \mathbf{M}^{-1}\mathbf{h}^{n}.$$

We refer the interested reader to [8] for implementation aspects.

4. Spectral analysis of the preconditioner

In this section we analyze the spectral properties of the proposed preconditioner by means of Fourier analysis, and for sake of notation, we drop hereafter the time index. We consider an unbounded domain $\Omega \equiv \mathbb{R}^3$ and we assume the fibers to be parallel (*i.e.* $\boldsymbol{a}_\tau$, $\tau = l, t, n$, are independent of $\mathbf{x}$). We assume, without loss of generality, the reference frame to have the first component aligned with the longitudinal axis of the fibers, so that, owing to (2), the diffusion tensors are diagonal. We assume that the intra and extracellular media are homogenous (*i.e.* $\sigma_\tau^{l,t,n}$, $\tau = i, e$, are independent of $\mathbf{x}$). We introduce the continuous operators $\mathcal{B} : [H^1(\Omega)]^2 \to [H^{-1}(\Omega)]^2$ and $\mathcal{M} : [H^1(\Omega)]^2 \to [H^{-1}(\Omega)]^2$, associated with problems (8) and with the semi-discrete counterpart of (11). With these positions, the asymptotic requirements for the Fourier transformability of the extracellular potential automatically fix the arbitrary function of time ([23]). We denote by k_1, k_2 and k_3 the dual frequency variables, and the Fourier transform of $w(x, y, z) = u(x, y, z), u_e(x, y, z)$ reads

$$\mathcal{F} : w(x, y, z) \mapsto \widehat{w}(k_1, k_2, k_3) = \int_{\mathbb{R}^3} e^{-i(k_1 x + k_2 y + k_3 z)} w(x, y, z)\, dxdydz.$$

The action of $\mathcal{B}$ and $\mathcal{M}$ can now be expressed for any $u \in [H^1(\Omega)]^2$ by means of the inverse Fourier transform, namely

$$\mathcal{B}u = \mathcal{F}^{-1}\left(B\widehat{u}\right) \qquad\qquad \mathcal{M}u = \mathcal{F}^{-1}\left(M\widehat{u}\right)$$

where B and M are the symbols of the operators $\mathcal{B}$ and $\mathcal{M}$, respectively. We denote by $(f, g)^T$ the right hand side in (8), and we let $\boldsymbol{k}^2 = k_2^2 + k_3^2$ as a consequence of assumption (2).
Considering $|k_1| < k_1^M$ and $|\boldsymbol{k}| < \boldsymbol{k}^M$, where k_1^M and $\boldsymbol{k}^M$ represent the maximal frequencies supported by the numerical grid (of order π/h, h being the mesh size), we introduce the modulated spatial frequencies $\xi = \sigma_i^l k_1^2 + \sigma_i^t \boldsymbol{k}^2$, and $\eta = \sigma_e^l k_1^2 + \sigma_e^t \boldsymbol{k}^2$, and we analyze the effectiveness of the preconditioning operator over the domain

$$T = \{\lambda_M \xi - c_1 \le \eta \le \lambda_M \xi,\ \lambda_m \xi \le \eta \le \lambda_m \xi + c_2\} \setminus \{(0, 0)\}, \tag{12}$$

shown in Figure 1, where c_1 and c_2 are positive constants depending on $k_1^M, \boldsymbol{k}^M$ and on the conductivity values. As k_1^M and $\boldsymbol{k}^M$ tend to infinity (and $h \to 0$), the domain T covers the angular sector $S = \{\lambda_m \xi \le \eta \le \lambda_M \xi\} \setminus \{(0, 0)\}$.
The preconditioned Bidomain problem reads then, in the frequency domain:

$$[M(\xi, \eta)]^{-1} B(\xi, \eta) \begin{bmatrix} \widehat{u} \\ \widehat{u}_e \end{bmatrix} = [M(\xi, \eta)]^{-1} \begin{bmatrix} \Delta t \widehat{f} \\ \widehat{g} \end{bmatrix}$$

where

$$B(\xi, \eta) = \begin{bmatrix} \chi C_m + \Delta t \frac{\lambda}{1+\lambda}\xi & \Delta t \left[\frac{\lambda}{1+\lambda}\xi - \frac{1}{1+\lambda}\eta\right] \\ \xi & \xi + \eta \end{bmatrix} \tag{13}$$

and

$$M(\xi, \eta) = \begin{bmatrix} \chi C_m + \Delta t \frac{\lambda}{1+\lambda}\xi & 0 \\ \xi & \xi + \eta \end{bmatrix}. \tag{14}$$

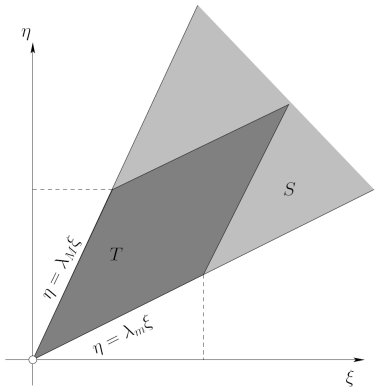

FIGURE 1. The domains T and S.

For $(\xi,\eta) \neq (0,0)$ the matrix $M(\xi,\eta)$ is invertible. From now on we set $\chi C_m = 1$, as this is the standard assumption in the applications (see [6]).
With these notations, the preconditioned operator reads

$$P(\xi,\eta) = [M(\xi,\eta)]^{-1} B(\xi,\eta) = \begin{bmatrix} 1 & \alpha(\xi,\eta) \\ 0 & 1 - \dfrac{\xi}{\xi+\eta}\alpha(\xi,\eta) \end{bmatrix}, \tag{15}$$

where

$$\alpha(\xi,\eta) = \frac{\Delta t}{1+\lambda} \; \frac{[\lambda\,\xi - \eta]}{1 + \frac{\lambda}{1+\lambda}\,\Delta t\,\xi}. \tag{16}$$

The eigenvalues of $P(\xi,\eta)$ are given by its diagonal entries, and we let

$$\gamma(\xi,\eta) = 1 - \frac{\xi}{\xi+\eta}\alpha(\xi,\eta) = \frac{1 + \Delta t\xi \, \dfrac{1}{\frac{\xi}{\eta}+1}}{1 + \Delta t\xi \, \dfrac{1}{\frac{1}{\lambda}+1}}. \tag{17}$$

In [8] it has ben proven that

$$\gamma_m(\lambda) = \frac{\frac{1}{\lambda}+1}{\frac{1}{\lambda_m}+1} \leq \gamma(\xi,\eta) \leq \frac{\frac{1}{\lambda}+1}{\frac{1}{\lambda_M}+1} = \gamma_M(\lambda). \tag{18}$$

We let $K_\gamma = \frac{\gamma_M(\lambda)}{\gamma_m(\lambda)}$, and we obtain from (18) that for all $\lambda_m \leq \lambda \leq \lambda_M$

$$1 < K_\gamma = \left(1 + \frac{1}{\lambda_M}\right)^{-1} \left(1 + \frac{1}{\lambda_m}\right). \tag{19}$$

Notice that, though defined as the ratio between $\gamma_M(\lambda)$ and $\gamma_m(\lambda)$, K_γ is actually a constant that does not depend on λ, but only on the conductivity coefficients. The spectrum of the preconditioned operator is then bounded independently of the choice $\lambda \in [\lambda_m, \lambda_M]$. Moreover, we recall that the maximal frequency supported by a numerical grid is of the order π/h. Since K_γ does not depend on the Fourier variables either, the spectrum of the preconditioned operator is also bounded independently of the frequencies, and thus of the mesh size.
Finally, we can observe from (18) that, if $\lambda = \lambda_m$ all the eigenvalues are bigger than 1 and bounded

from above, if $\lambda = \lambda_M$ all the eigenvalues are smaller than 1 and bounded away from 0, while for $\lambda_m < \lambda < \lambda_M$ the eigenvalues cluster around 1 (see [8]). Using the values for σ_τ^l and σ_τ^t proposed in [5], we get $\lambda_m = 0.6667$ and $\lambda_M = 4.2868$, and we have $K_\gamma \leq 2.0259$.

4.1. **Conditioning of the preconditioned problem.** The matrix $P(\xi,\eta)$ of the preconditioned problem is non symmetric. For this reason, K_γ is just a rough estimate of its conditioning, and we therefore estimate it here from the analysis of its singular values, which are given by

$$\sigma_P^{\pm}(\xi,\eta) = \sqrt{\psi^{\pm}(\xi,\eta)},$$

$\psi^{\pm}(\xi,\eta)$ being the eigenvalues of the matrix

$$Y(\xi,\eta) = [P(\xi,\eta)]^T P(\xi,\eta) = \begin{bmatrix} 1 & \alpha(\xi,\eta) \\ \alpha(\xi,\eta) & [\gamma(\xi,\eta)]^2 + [\alpha(\xi,\eta)]^2 \end{bmatrix}.$$

Owing to (17), we have

$$\alpha(\xi,\eta) = \left(1 + \frac{\eta}{\xi}\right)\left[1 - \gamma(\xi,\eta)\right],$$

and the eigenvalues of $Y(\xi,\eta)$ are given by

$$\psi^{\pm}(\xi,\eta) = \frac{1}{2}\left[1 + [\gamma(\xi,\eta)]^2 + \left(1+\frac{\eta}{\xi}\right)^2\left(1-\gamma(\xi,\eta)\right)^2\right]$$

(20)
$$\pm\frac{1}{2}\sqrt{\left[1 + [\gamma(\xi,\eta)]^2 + \left(1+\frac{\eta}{\xi}\right)^2\left(1-\gamma(\xi,\eta)\right)^2\right]^2 - 4[\gamma(\xi,\eta)]^2}$$

We now focus on $\psi^+(\xi,\eta)$ and $\psi^-(\xi,\eta)$: both are real positive and we have $0 < \psi^-(\xi,\eta) < \psi^+(\xi,\eta)$. Gathering together (20) and (18), and owing to the fact that $\lambda_m\xi \leq \eta \leq \lambda_M\xi$, we get an upper bound for the larger eigenvalue $\psi^+(\xi,\eta)$ given by

$$\psi^+(\xi,\eta) < 1 + \left[\gamma_M(\lambda)\right]^2 + \left(1+\lambda_M\right)^2\left[1-\gamma(\xi,\eta)\right]^2. \tag{21}$$

We now turn our attention on the term $[1-\gamma(\xi,\eta)]^2$: we have, from (16) and (17), $\gamma(\xi,\eta) < 1$ for $\eta < \lambda\xi$ and $\gamma(\xi,\eta) > 1$ for $\eta > \lambda\xi$, and

$$|1-\gamma(\xi,\eta)| = \begin{cases} 1-\gamma(\xi,\eta) \leq \left[\dfrac{1}{\frac{1}{\lambda}+1} - \dfrac{1}{\frac{1}{\lambda_m}+1}\right]\dfrac{\Delta t\xi}{1+\Delta t\xi\,\frac{1}{\frac{1}{\lambda}+1}} & \eta \leq \lambda\xi \\ \gamma(\xi,\eta)-1 \leq \left[\dfrac{1}{\frac{1}{\lambda_M}+1} - \dfrac{1}{\frac{1}{\lambda}+1}\right]\dfrac{\Delta t\xi}{1+\Delta t\xi\,\frac{1}{\frac{1}{\lambda}+1}} & \eta > \lambda\xi. \end{cases}$$

The common term in ξ is monotone increasing thus it can be bounded from above by its limit as $\xi \to \infty$:

$$\frac{\Delta t\xi}{1+\Delta t\xi\,\frac{1}{\frac{1}{\lambda}+1}} \leq \lim_{\xi\to\infty}\frac{\Delta t\xi}{1+\Delta t\xi\,\frac{1}{\frac{1}{\lambda}+1}} = \frac{1}{\lambda}+1.$$

Thus we have from (18)

$$|1-\gamma(\xi,\eta)| \leq \max\left[\gamma_M(\lambda)-1\ ,\ 1-\gamma_m(\lambda)\right],$$

and the upper bound for $\psi^+(\xi,\eta)$ is given by:

$$\psi^+(\xi,\eta) < 1 + [\gamma_M(\lambda)]^2 + [1+\lambda_M]^2 \max\left([\gamma_M(\lambda)-1]^2\ ,\ [1-\gamma_m(\lambda)]^2\right) = \psi^+_*(\lambda). \tag{22}$$

We now turn to estimate the minimum of $\psi^-(\xi,\eta)$. Since $\det(P^TP) = \gamma^2$, we have

$$\psi^-(\xi,\eta) = \frac{[\gamma(\xi,\eta)]^2}{\psi^+(\xi,\eta)},$$

thus the minimum eigenvalue $\psi^-(\xi,\eta)$ is bounded from below by

$$\psi^-(\xi,\eta) \geq \frac{[\gamma_m(\lambda)]^2}{\psi^+_*(\lambda)} \tag{23}$$

where $\gamma_m(\lambda)$ is defined in (18). We can thus conclude that the effective conditioning of the continuous preconditioned problem is bounded from above by

$$\kappa_2(P) = \frac{\max_{(\xi,\eta)\in T}\sigma^+_P(\xi,\eta)}{\min_{(\xi,\eta)\in T}\sigma^-_P(\xi,\eta)} = \frac{\max_{(\xi,\eta)\in T}\sqrt{\psi^+(\xi,\eta)}}{\min_{(\xi,\eta)\in T}\sqrt{\psi^-(\xi,\eta)}} \leq \frac{\psi^+_*(\lambda)}{\gamma_m(\lambda)}$$

and eventually we get

$$\kappa_2(P) \leq K_\gamma + K_\gamma^2 + [1+\lambda_M]^2\ K_\gamma \max\left([\gamma_M(\lambda)-1]^2\ ,\ [1-\gamma_m(\lambda)]^2\right) = K(\lambda), \tag{24}$$

being again $K_\gamma = \gamma_M/\gamma_m$. As the bound in (24) depends only on the coefficients of the problem and the parameter λ, we conclude that the conditioning of the preconditioned problem at the discrete level is independent of the mesh size h.

4.2. **Convergence for a Krylov method.** Since the matrix of the Bidomain problem is non symmetric, we use at the discrete level a Krylov type algorithm to solve its associated linear system. In this section we consider to solve the discrete version of the preconditioned operator $P(\xi,\eta)$ by GMRES. In the Fourier space, the matrix of right eigenvectors for $P(\xi,\eta)$ is given by

$$W(\xi,\eta) = \begin{bmatrix} 1 & -\dfrac{\alpha(\xi,\eta)}{1-\gamma(\xi,\eta)} \\ 0 & 1 \end{bmatrix} = \begin{bmatrix} 1 & -\dfrac{\xi+\eta}{\xi} \\ 0 & 1 \end{bmatrix},$$

where the last equality follows from the definition of $\gamma(\xi,\eta)$ (17). The matrix $W(\xi,\eta)$ is invertible, thus the residual norm $\|r_m\|_2$ achieved by the m-th step of the GMRES algorithm satisfies

$$\|r_m\|_2 \leq \kappa_2(W)\epsilon^{(m)}\|r_0\|_2,$$

where $\|r_0\|_2$ is the initial residual norm, $\kappa_2(W)$ is the conditioning of the matrix of eigenvectors, and where $\epsilon^{(m)}$ depends on the eigenvalues of the preconditioned problem ([25], Proposition 6.15).
Conditioning of the Eigenvectors matrix. The matrix $W(\xi,\eta)$ being non symmetric, we compute its conditioning by means of its singular values. We have:

$$X(\xi,\eta) = [W(\xi,\eta)]^T W(\xi,\eta) = \begin{bmatrix} 1 & -\dfrac{\xi+\eta}{\xi} \\ -\dfrac{\xi+\eta}{\xi} & 1+\left[\dfrac{\xi+\eta}{\xi}\right]^2 \end{bmatrix}.$$

The matrix $X(\xi,\eta)$ and its eigenvalues have to be evaluated on the domain T (see Figure 1): we can change variables and express the matrix $X(\xi,\eta)$ in terms of (ξ,λ), with $\lambda_m \leq \lambda \leq \lambda_M$. Along the line $\eta = \lambda\xi$, we have

$$\frac{\xi+\eta}{\xi} = 1+\lambda,$$

and, we reduce ourselves to analyze the eigenvalues of :

$$X(\xi,\lambda) = \begin{bmatrix} 1 & -[1+\lambda] \\ -[1+\lambda] & 1+[1+\lambda]^2 \end{bmatrix}.$$

Since $det\, X(\xi,\lambda) = 1$ and $tr\, X(\xi,\lambda) = 2+[1+\lambda]^2$, the eigenvalues of the matrix $X(\xi,\lambda)$ solve, for any given $\lambda \in [\lambda_m, \lambda_M]$, the equation

$$(\mu-1)^2 = [1+\lambda]^2\mu, \tag{25}$$

and depend on λ only. Equation (25) has always two positive roots (see Figure 2), which are given

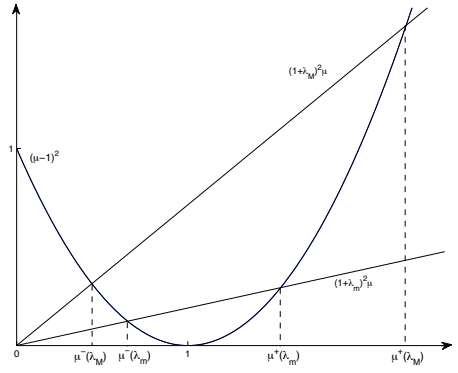

FIGURE 2. Eigenvalues location for $X(\xi,\lambda)$: slopes modified for visualization purpose.

by

$$\mu^{\pm}(\lambda) = \frac{1}{2}\left[2+(1+\lambda)^2 \pm (1+\lambda)\sqrt{(1+\lambda)^2+4}\right],$$

while the singular values of the matrix $W(\xi,\lambda)$ are $\sigma_W^{\pm}(\lambda) = \sqrt{\mu^{\pm}(\lambda)}$.
Moreover, since $\mu^+(\lambda)\mu^-(\lambda) = 1$ for all λ, and $\mu^+(\lambda) > 1$ is increasing in λ, the conditioning of the eigenvectors matrix $W(\xi,\eta)$ is given by

$$\kappa_2(W) = \max_{\lambda_m \le \lambda \le \lambda_M} \frac{\sqrt{\mu^+(\lambda)}}{\sqrt{\mu^-(\lambda)}} = \max_{\lambda_m \le \lambda \le \lambda_M} \mu^+(\lambda) = \mu^+(\lambda_M). \tag{26}$$

The conditioning of the eigenvectors matrix, being independent from the frequency variables (ξ,η), is thus independent from the mesh size h, and, with the coefficients of the problem proposed in [5], we get $\kappa_2(W) = 29.8449$.

Estimation of $\epsilon^{(m)}$. If the spectrum of the preconditioned matrix is contained in an ellipse of the complex plane with center c, focal distance d and and major semi axis a, not containing the origin, $\epsilon^{(m)}$ is given in terms of Chebyshev polynomials of order m, and can be approximated (see [25]) by

$$\epsilon^{(m)} = \frac{C_m\left(\frac{a}{d}\right)}{\left|C_m\left(\frac{c}{d}\right)\right|} \approx \left(\frac{a+\sqrt{a^2-d^2}}{c+\sqrt{c^2-d^2}}\right)^m.$$

We proved in the previous section that the eigenvalues of the preconditioned problem are real and bounded away from 0. The spectrum is thus contained in a degenerate ellipse, the interval

$[\gamma_m, \gamma_M]$, where γ_m and γ_M are the ones defined in (18): the dependence on λ is understood in this section. With these positions, we have $a = d = \frac{\gamma_M - \gamma_m}{2}$, $c = \frac{\gamma_M + \gamma_m}{2}$, and we get

$$\epsilon^{(m)} \approx \left(\frac{a}{c + \sqrt{c^2 - d^2}} \right)^m = \left(\frac{\gamma_M - \gamma_m}{\gamma_M + \gamma_m + \sqrt{(\gamma_M + \gamma_m)^2 - (\gamma_M - \gamma_m)^2}} \right)^m$$

$$= \left(\frac{\gamma_M - \gamma_m}{\gamma_M + \gamma_m + 2\sqrt{\gamma_M \gamma_m}} \right)^m = \left(\frac{\gamma_M - \gamma_m}{(\sqrt{\gamma_M} + \sqrt{\gamma_m})^2} \right)^m = \left(\frac{\sqrt{\gamma_M} - \sqrt{\gamma_m}}{\sqrt{\gamma_M} + \sqrt{\gamma_m}} \right)^m.$$

Since $\gamma_m > 0$, we can conclude

$$\epsilon^{(m)} \approx \left(\frac{\sqrt{K_\gamma} - 1}{\sqrt{K_\gamma} + 1} \right)^m, \tag{27}$$

where, again, $K_\gamma = \gamma_M / \gamma_m$. Owing to (19), the above quantity is then bounded independently of both the Fourier variables (and thus from the mesh parameter) and λ, and with the coefficients of the problem proposed in [5] we get $\epsilon \approx 0.1748$.

Remark 4.1. *If the preconditioned matrix were symmetric, the quantity K_γ would be its condition number, and estimate* (27) *would be the reduction factor of the conjugate gradient (CG) method. Since all the eigenvalues are real (and positive) a non-standard inner product induced by the preconditioned matrix P exists, $\langle x, y \rangle_P = x^T A(P) y$, with respect to which P itself is symmetric positive definite. A CG method based on $\langle \cdot, \cdot \rangle_P$ could possibly be more convenient than the use of the GMRES in terms of memory requirements, provided $A(P)$ is simple enough. This aspect will be the subject of a susequent investigation, that will be carried out directly at the discrete level.*

4.3. **Optimization of the parameter λ.** We proved that the preconditioner is robust with respect to the mesh size since, for any choice of the parameter $\lambda \in [\lambda_m, \lambda_M]$, the conditioning of the eigenvectors matrix $\kappa_2(W)$, the reduction factor $\epsilon^{(m)}$, the conditioning of the preconditioned problem $\kappa_2(P)$, and the parameter K_γ are bounded independently of the frequency variables (ξ, η). We are now interested in optimizing the preconditioner performances with respect to λ. To this extent, we notice that $\kappa_2(W)$ and $\epsilon^{(m)}$ are estimated by quantities depending on λ_m and λ_M only, while the upper bound for $\kappa_2(P)$ is a function of λ.
The only possible choice to optimize the preconditioner performances is thus given by minimizing the upper bound on the condition number of the preconditioned matrix $P(\xi, \eta)$. This amounts to identify λ^* as the solution of the minimization problem

$$K(\lambda^*) = \min_{\lambda \in [\lambda_m, \lambda_M]} K(\lambda). \tag{28}$$

First, notice that, owing to the definition of K_γ and (19), the function $K(\lambda)$ can be rewritten as

$$K(\lambda) = K_\gamma + K_\gamma^2 + K_\gamma \max\left[\phi_1(\lambda), \phi_2(\lambda)\right],$$

where we have set

$$\phi_1(\lambda) = \left[1 - \frac{\lambda_M}{\lambda}\right]^2 \qquad \phi_2(\lambda) = \left[\frac{1 + \lambda_M}{1 + \lambda_m}\right]^2 \left[1 - \frac{\lambda_m}{\lambda}\right]^2.$$

We have, for all $\lambda \in [\lambda_m, \lambda_M]$,

$$\phi_1'(\lambda) = 2\left[1 - \frac{\lambda_M}{\lambda}\right] \frac{\lambda_M}{\lambda^2} < 0 \qquad \phi_2'(\lambda) = 2\left[\frac{1 + \lambda_M}{1 + \lambda_m}\right]^2 \left[1 - \frac{\lambda_m}{\lambda}\right] \frac{\lambda_m}{\lambda^2} > 0.$$

Moreover, since

$$\phi_1(\lambda_m) > 0 \qquad \phi_1(\lambda_M) = 0 \qquad \phi_2(\lambda_m) = 0 \qquad \phi_2(\lambda_M) > 0,$$

the minimum of $K(\lambda)$ is attained at the intersection of the two curves $\phi_1(\lambda^*) = \phi_2(\lambda^*)$.
A simple algebra provides

$$\lambda^* = \frac{\lambda_m + \lambda_M + 2\lambda_m\lambda_M}{2 + \lambda_m + \lambda_M}. \tag{29}$$

In Figure 3 we plot the upper bound on the effective condition number as a function of λ: the coefficients of the problem are the ones proposed in [5].

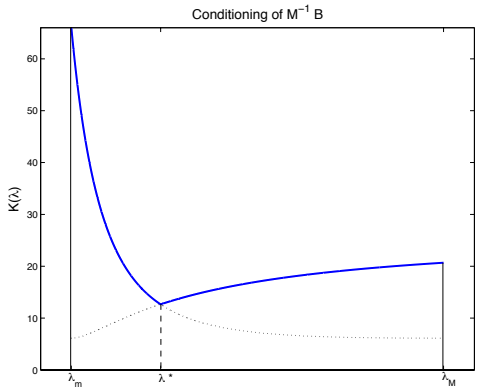

FIGURE 3. Upper bound on the conditioning of the preconditioned problem $K(\lambda)$.

Remark 4.2. *By inserting the parameter λ^* identified in* (29) *into* (18)*, we get*

$$1 - \gamma_m(\lambda^*) = \gamma_M(\lambda^*) - 1,$$

namely λ^* provides an upper and a lower bound to the eigenvalues clustering of the preconditioned problem that are symmetric with respect to 1. With the coefficients proposed in [5]*, we get $\lambda^* = 1.5344$, $\gamma_m(\lambda^*) = 0.661$, and $\gamma_M(\lambda^*) = 1.339$.*

5. The case $\lambda \to +\infty$

If we let the coefficient λ go to $+\infty$ in (7), we recover the Parabolic-Elliptic (PE) symmetric formulation

$$\begin{cases} \chi C_m \dfrac{\partial u}{\partial t} - \nabla \cdot \mathbf{D}_i \nabla u - \nabla \cdot \mathbf{D}_i \nabla u_e + \chi I_{ion}(u) = I^{\text{app}} \\ \\ -\nabla \cdot \mathbf{D}_i \nabla u - \nabla \cdot (\mathbf{D}_i + \mathbf{D}_e) \nabla u_e = \widetilde{I}^{\text{app}}, \end{cases} \tag{30}$$

widely used in the Biongineering community. Keeping the same notations as in Section 3, the associated matrix at the discrete level is given by

$$\begin{bmatrix} \dfrac{\chi C_m}{\Delta t}\mathcal{M} + \mathcal{K}_i & \mathcal{K}_i \\ \\ \mathcal{K}_i & \mathcal{K}_i + \mathcal{K}_e \end{bmatrix}$$

The block triangular preconditioner can be defined also in this case, and in the rest of the section we outline its spectral analysis. An argument similar to the one in Section 4.1 shows that the

PE-Bidomain problem is represented, in the frequency domain, by the matrix

$$B(\xi,\eta) = \begin{bmatrix} \dfrac{\chi C_m}{\Delta t} + \xi & \xi \\ \xi & \xi + \eta \end{bmatrix}.$$

Notice that, although in this case $\lambda \to +\infty$, we still analyze the effectiveness of the preconditioner, in the frequency domain, over the set T defined in (12). A simple algebra shows that the matrix $P(\xi,\eta)$ of the lower block-triangular preconditioned problem has the same form as in (15), where in this case we have

$$\alpha = \frac{\Delta t\, \xi}{1 + \Delta t\, \xi},$$

and, as usual, we have assumed $\chi C_m = 1$. Since $0 \leq \alpha < 1$, the eigenvalues of the preconditioned problem are either 1 or bounded by

$$\frac{1}{\frac{1}{\lambda_m} + 1} \leq \gamma(\xi,\eta) < 1. \tag{31}$$

5.1. **Conditioning of the preconditioned problem.** The structure of the preconditioned matrix being the same as in Section 4.1, the same procedure and (31) entail the following bound on the singular values of the preconditioned problem:

$$\psi^+(\xi,\eta) \;<\; 1 + [\gamma(\xi,\eta)]^2 + \left(1 + \frac{\xi}{\eta}\right)[1 - \gamma(\xi,\eta)]^2 \;<\; 2 + \left[\frac{1+\lambda_M}{1+\lambda_m}\right]^2.$$

As a consequence, the effective conditioning of the preconditioned problem is bounded from above by

$$\kappa_2(P) \leq 2\left(1 + \frac{1}{\lambda_m}\right) + \frac{[1+\lambda_M]^2}{\lambda_m(1+\lambda_m)}. \tag{32}$$

Also in this case, since the bound in (32) does not depend on the frequency variable, we conclude that the conditioning at the discrete level is bounded independently of the mesh size h.
With the coefficients proposed in [5], we get $\kappa_2(P) \leq 30.1533$.

5.2. **Convergence for a Krylov method.** The formal structure of the preconditioned matrix $P(\xi,\eta)$, as well as the relation between $\alpha(\xi,\eta)$ and $\gamma(\xi,\eta)$ are the same as the ones in Section 4.2. As a consequence, the results obtained in Section 4.2 still hold when the block-triangular preconditioner is applied to the the PE-Bidomain problem (30).

6. Numerical results

In this section we present some numerical results in 3D to study the optimality of the parameter λ^*, identified in the previous section, that minimizes the upper bound on the conditioning of the preconditioned problem. We test the optimality of λ^* with respect to mesh size, time step and ionic model. We do not compare here the preconditioner performances with respect to other preconditioners available in literature as such comparison, together with an extensive analysis of the preconditioner performances has already been the subject of the numerical tests presented in [8].
The computational domain is either a real ventricular geometry reconstructed from SPECT images or the ellipsoid introduced, with an analytical description of the fiber orientation, in [5] (see Figure 4). We use as ionic models both the Rogers-McCulloch variant of the FitzHugh-Nagumo (**RM**), and the Luo-Rudy Phase 1 (**LR1**) model. The numerical tests are carried out with `LifeV` [1], a finite element library using the `Trilinos` packages `BELOS` and `IFPACK` [2]. The discrete problem is

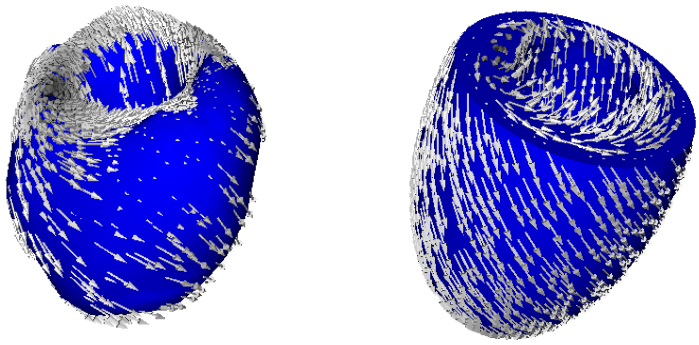

FIGURE 4. The computational domains. Left: real ventricular geometry reconstructed from SPECT images. Right: ellipsoidal geometry introduced in [5]. White arrows represent myocardial fiber orientation used in our numerical simulations.

solved with a Flexible GMRES preconditioned on the right: this allows to solve the linear system in the preconditioning step by an iterative method with a coarse tolerance (see [8] for implementation details). The stopping criterion is based on the 2-norm of the current residual, normalized with respect to the 2-norm of the initial residual, and the tolerance is set to 10^{-5}. The preconditioner is expected to be fairly independent from the mesh size. Moreover, since the eigenvector matrix for the preconditioned problem features a good conditioning independently of the parameter λ, we expect also reasonably good performances for any choice of $\lambda \in [\lambda_m, \lambda_M]$. We consider different values of λ: the two endpoints, λ_m and λ_M, the optimized parameter λ^*, and the medium points $\lambda_{m,*} = (\lambda_m + \lambda^*)/2$ and $\lambda_{M,*} = (\lambda^* + \lambda_M)/2$. Relying on the coefficients proposed in [5], we thus consider the values

$$\lambda_m = 0.6667 \qquad \lambda_{m,*} = 1.1006 \qquad \lambda^* = 1.5344 \qquad \lambda_{*,M} = 2.91 \qquad \lambda_M = 4.2868$$

We also consider $\lambda = 1.3$, the value used in [8] and therein tuned in an empirical way.

6.1. **Influence of the mesh size.** For this test we use the realistic ventricular geometry and different mesh sizes. The ionic model is the Rogers-McCulloch. We use a time step of $\Delta t = 0.5$ ms, and we simulate, for different mesh sizes and different values of λ, the first 50ms of the action potential propagation: during this phase the depolarization front is traveling in the computational domain, making the Bidomain simulation computationally more expensive. We report in Table

TABLE 1. Ventricular geometry **RM** ionic model: average iteration counts per time step for different mesh sizes, and for various values of λ.

λ	λ_m	$\lambda_{m,*}$	λ^*	$\lambda_{*,M}$	λ_M	1.3
# nodes	iter	iter	iter	iter	iter	iter
22,470	6.06	5.02	5.04	6.02	6.09	5.0
58,943	7.23	6.01	6.01	6.46	7	6.01
156,733	8.04	6.88	6.12	6.08	7.01	6.22
276,578	7.26	6.03	6.00	6.07	6.98	6.01
677,000	7.99	6.08	6.05	7.00	7.06	6.06

1 the average iteration counts for the different values of λ and for different mesh sizes. The preconditioner shows its fair insensitiveness with respect to the mesh size also for a real geometry in the presence of a complex fibers distribution, even if its derivation has been carried out in the special case where the fibers are aligned with the cartesian axes. The performance of the parameter λ^* shows an evident stability as the mesh size decreases, which can be expected, since it has been derived in a continuous framework.

6.2. **Influence of the time step.** In the second series of tests, the computational domain is still the ventricular geometry, and the ionic model is the Rogers-McCulloch one. We use the largest mesh (677,000 nodes) of the previous section. In order to assess the behavior of the preconditioner in the three principal phases of the action potential (depolarization, plateau, repolarization) we consider here longer simulation of 400ms, sufficient to include a whole heartbeat. We test the sensitivity of the parameter λ^* with respect to the time step, by choosing three different values: $\Delta t = 0.5, 0.25, 0.125$. We report in Table 2 the average iteration counts per time step and the average CPU time (in seconds) to solve the linear system within each time step, for the different values of λ and the different time steps.

TABLE 2. Ventricular mesh with 677,000 dof, **RM** ionic model: average iteration counts and CPU time (in s) per time step over 400ms, for various values of λ and different time step Δt.

	λ	λ_m	$\lambda_{m,*}$	λ^*	$\lambda_{*,M}$	λ_M	1.3
$\Delta t = 0.5$	iter	7.20875	6.02125	6.00625	7	7.09625	6.0075
	CPU	191.377	165.131	172.919	198.332	197.179	165.302
$\Delta t = 0.25$	iter	6.25312	5.04625	5.01187	6.005	6.25938	5.04812
	CPU	180.454	147.761	150.268	200.183	196.094	157.449
$\Delta t = 0.125$	iter	7.00063	6	5.97	5.04437	5.88969	6
	CPU	199.607	151.44	144.588	163.344	193.371	177.434

We observe that the preconditioner shows fair insensitiveness, for all values of λ considered, with respect to the time step. In addition, the optimality of λ^* becomes significantly evident in terms of computational cost, as the time step Δt gets smaller. Moreover, the CPU time associated with the parameter λ^* is consistently decreasing with the time step, while the other values of λ feature a more erratic behavior.

6.3. **Influence of the ionic model.** In this last series of tests, the computational domain is the ellipsoid with analytical fibers description, introduced in [5] and discretized by a tetrahedral mesh with 578,442 nodes. For the different values of λ, we simulate 450ms of propagation using both the Rogers-McCulloch and the Luo-Ruody phase one **LR1** ionic models. The time step is $\Delta t = 0.5$ms for the **RM** model, and $\Delta t = 0.1$ for the **LR1** model, as the latter requires a smaller time step in order to handle the stiffness of the upstroke part of the action potential. The computed averages are thus based on 900 and 4500 time steps, respectively. We again report in Table 3 the average iteration counts per time step and the average CPU time (in seconds) to solve the linear system within each time step, for the different values of λ and the different ionic models. We can infer from Table 3 the robustness of the preconditioner with respect to the ionic model, for the various values of λ. Moreover, as it can be expected from the tests in the previous section, the parameter λ^* performs better with the Luo-Rudy Phase 1 model, as the time step for this model is smaller than the time step for the Rogers-McCulloch one.

TABLE 3. Ellipsoidal mesh with 578,442 dof: average iteration counts and CPU time (in s) per time step over 450ms, for various values of λ and different ionic models.

	λ	λ_m	$\lambda_{m,*}$	λ^*	$\lambda_{*,M}$	λ_M	1.3
RM	iter	9.07	7.0256	7	7	7.	7.0011
	CPU	211.409	168.67	184.115	217.687	241.374	173.622
LR1	iter	7.33889	6.99667	5.08756	6.0566	6.1089	5.1391
	CPU	126.789	125.959	105.188	151.993	177.203	126.088

7. Conclusions

We analyzed in this paper the spectral properties of the model-based block-triangular preconditioner introduced in [8]. By minimizing an upper bound on the conditioning of the preconditioned problem, we identified an optimal parameter λ^*, for which we provide an explicit formula. Involving only the coefficient of the problem, such formula can easily be used in implementations. Although the analysis and the optimization have been performed in the very special case where the fibers are aligned with the reference axes, numerical tests on a both a real ventricular geometry reconstructed from SPECT imaging, and an analytical ellipsoidal geometry described in [5], are in good agreement with the conclusions of the analysis itself. In particular, the upper bound on the conditioning of the preconditioned problem being dependent only on the coefficients of the problem, the preconditioner turns out to be fairly insensitive to the mesh size, the time step and the ionic model used, for all suitable choices of the parameter λ. Moreover, the numerical tests show that the performances of the preconditioner associated with the value λ^* improve with the reduction of the mesh size and the time step, confirming the asymptotic optimality of the proposed parameter.

Acknowledgements. The authors thank Umberto Villa (Emory University) for some fruitful discussions in the preparation of this work.

References

[1] `LifeV` software. *http://www.LifeV.org*.
[2] `Trilinos` software. *http://trilinos.sandia.gov*.
[3] N. Ayache, editor. *Computational Models for the Human Body*, chapter Computational Methods fro Cardiac Electrophysiology - by M.E. Belik, T.P. Usyk, A.D. McCulloch. Handbook of Numerical Analysis. Elsevier North Holland, 2004.
[4] P. Colli Franzone, P. Deuflhard, B. Erdmann, J. Lang, and L.F. Pavarino. Adaptivity in space and time for reaction-diffusion systems in electrocardiology. *SIAM Journal on Scientific Computing*, 28(3):942–962, 2006.
[5] P. Colli Franzone and L. F. Pavarino. A parallel solver for reaction-diffusion systems in computational electrocardiology. *Mathematical models and methods in applied sciences*, 14(6):883–911, 2004.
[6] P. Colli Franzone, L. F. Pavarino, and B. Taccardi. Simulating patterns of excitation, repolarization and action potential duration with cardiac Bidomain and Monodomain models. *Math. Biosc.*, 197:35–66, 2005.
[7] P. Colli Franzone and G. Savaré. Degenerate evolution systems modeling the cardiac electric field at micro and macroscopic level. In A. Lorenzi and B. Ruf, editors, *Evolution Equations, Semigroups and Functional Analysis*, pages 49–78. Birkhauser, 2002.
[8] L. Gerardo-Giorda, L. Mirabella, F. Nobile, M. Perego, and A. Veneziani. A model-based block-triangular preconditioner for the Bidomain system in electrocardiology. *J. Comp. Phys.*, 228:3625–3639, 2009.
[9] S. H. Gilbert, A. P. Benson, P. Li, and A. V. Holden. Regional localisation of left ventricular sheet structure: integration with current models of cardiac fibre, sheet and band structure. *European Journal of Cardio-Thoracic Surgery*, 32(2):231–249, August 2007.
[10] C.S. Henriquez. Simulating the electrical behavior of cardiac tissue using the bidomain model. *Crit. Rev. Biomed. Engrg.*, 21:1–77, 1993.

[11] N. Hooke, C. S Henriquez, P. Lanzkron, and D. Rose. Linear algebraic transformations of the bidomain equations: Implications for numerical methods. *Mathematical Biosciences*, 120(2):127–145, 1994. 0025-5564 doi: DOI: 10.1016/0025-5564(94)90049-3.
[12] J. Le Grice, B.H. Smaill, and P.J. Hunter. Laminar structure of the heart: a mathematical model. *Am. J. Physiol.*, 272 (Heart Circ. Physiol.)(41):H2466–H2476, 1995.
[13] M. Munteanu, L. F. Pavarino, and S. Scacchi. A scalable newton–krylov–schwarz method for the bidomain reaction-diffusion system. *SIAM Journal on Scientific Computing*, 31(5):3861–3883, 2009.
[14] L. F. Pavarino and S. Scacchi. Multilevel additive Schwarz preconditioners for the Bidomain reaction-diffusion system. *SIAM J. Sci. Comp.*, 31(1):420–443, 2008.
[15] M. Pennacchio, G. Savarè, and P. Colli Franzone. Multiscale modelling for the bioelectric activity of the heart. *SIAM Journal on Mathematical Analysis*, 37(4):1333–1370, 2006.
[16] M. Pennacchio and V. Simoncini. Efficient algebraic solution of rection-diffusion systems for the cardiac excitation process. *J. Comput. Appl. Math.*, 145(1):49–70, 2002.
[17] M. Pennacchio and V. Simoncini. Algebraic multigrid preconditioners for the bidomain reactiondiffusion system. *Appl. Num. Math.*, 59(12):3033–3050, 2009.
[18] M. Perego and A. Veneziani. An efficient generalization of the Rush-Larsen method for solving electro-physiology membrane equations. *ETNA*, 35:234–256, 2009.
[19] A.J. Pullan, M.L. Buist, and L.K. Cheng. *Mathematical Modelling the Electrical Activity of the Heart*. World Scientific, Singapore, 2005.
[20] A. Quarteroni, L. Formaggia, and A. Veneziani, editors. *Complex Systems in Biomedicine*, chapter Computational electrocardiology: mathematical and numerical modeling - by P. Colli Franzone, L. Pavarino, G. Savaré. Springer, Milan, 2006.
[21] J. Rogers and A. McCulloch. A collocation-Galerkin finite element model of cardiac action potential propagation. *IEEE Transactions on Biomedical Engineering*, 41:743–757, 1994.
[22] B.J. Roth. Action potential propagation in a thick strand of cardiac muscle. *Circ. Res.*, 68:162–173, 1991.
[23] W. Rudin. *Real and Complex Analysis*. McGraw-Hill Science/Engineering/Math, 3 edition, May 1986.
[24] Y. Rudy and J.R. Silva. Computational biology in the study of cardiac ion channels and cell electrophysiology. *Quarter Reviews of Biophysics*, 39(1):57–116, 2006.
[25] Y. Saad. *Iterative Methods for Sparse Linear Systems*. PWS, Boston, 1996.
[26] F. B. Sachse. *Computational Cardiology*. Springer, Berlin, 2004.
[27] S. Scacchi. A hybrid multilevel Schwarz method for the bidomain model. *Computer Methods in Applied Mechanics and Engineering*, 197(45-48):4051–4061, August 2008.
[28] S. Scacchi. *Multilevel Schwarz preconditioner for the Bidomain system and applications in Electrocardiology*. PhD thesis, University of Pavia, 2008.
[29] M. Veneroni. Reaction-diffusion systems for the macroscopic bidomain model of the cardiac electric field. *Nonlinear Analysis: Real World Applications*, 10(2):849–868, April 2009.
[30] E.J. Vigmond, F. Aguel, and N.A. Trayanova. Computational techniques for solving the bidomain equations in three dimensions. *IEEE Trans. Biomed. Eng.*, 49(11):1260–1269, 2002.
[31] E.J. Vigmond, R. Weber dos Santos, A.J. Prassl, M. Deo, and G. Plank. Solvers for the caridac bidomain equations. *Progress in Biophysics and Molecular Biology*, 96(1-3):3–18, 2008.

BCAM - Basque Center for Applied Mathematics, Bilbao, Spain - lgerardo@bcamath.org

"Wallace H. Coulter" Dept. Biomedical Engnrg, GaTech, Atlanta, USA - lucia.mirabella@bme.gatech.edu